Structural properties of fluids interacting via piece-wise constant potentials with a hard core

Andrés Santos,[1, a)] Santos B. Yuste,[1, b)] Mariano López de Haro,[2, c)] Mariana Bárcenas,[3, d)] and Pedro Orea[4, e)]

[1)] *Departamento de Física, Universidad de Extremadura, Badajoz, E-06071, Spain*

[2)] *Instituto de Energías Renovables, Universidad Nacional Autónoma de México (U.N.A.M.), Temixco, Morelos 62580, Mexico*

[3)] *División de Ingeniería Química y Bioquímica, Tecnológico de Estudios Superiores de Ecatepec, Ecatepec, Edo. de México, 55210, Mexico*

[4)] *Programa de Ingeniería Molecular, Instituto Mexicano del Petróleo, México, D.F., 07730, Mexico*

(Dated: 16 April 2013)

The structural properties of fluids whose molecules interact via potentials with a hard core plus two piece-wise constant sections of different widths and heights are presented. These follow from the more general development previously introduced for potentials with a hard core plus n piece-wise constant sections [Condens. Matter Phys. **15**, 23602 (2012)] in which use was made of a semi-analytic rational-function approximation method. The results of illustrative cases comprising eight different combinations of wells and shoulders are compared both with simulation data and with those that follow from the numerical solution of the Percus–Yevick and hypernetted-chain integral equations. It is found that the rational-function approximation predicts a more accurate radial distribution function than the Percus–Yevick theory in all the cases and is comparable to or superior than the hypernetted-chain theory in most of the cases.

I. INTRODUCTION

Due to their relative simplicity, while having at the same time the ability to adequately account for diverse physical features of real fluids, discrete potentials of the form

$$\varphi(r) = \begin{cases} \infty, & r < \sigma, \\ \epsilon_1, & \sigma < r < \lambda_1\sigma, \\ \epsilon_2, & \lambda_1\sigma < r < \lambda_2\sigma, \\ \vdots & \vdots \\ \epsilon_n, & \lambda_{n-1}\sigma < r < \lambda_n\sigma, \\ 0, & r > \lambda_n\sigma, \end{cases} \tag{1}$$

have received some attention in the recent literature.[1–21] They comprise a hard core of diameter σ and n steps of "heights" ϵ_j and widths $(\lambda_j - \lambda_{j-1})\sigma$, with $\lambda_0 = 1$, so that $\lambda_n\sigma$ denotes the total range of $\varphi(r)$. The sign of ϵ_j determines whether the jth step is either a "shoulder" ($\epsilon_j > 0$) or a "well" ($\epsilon_j < 0$). The interaction potential at $r = \lambda_j\sigma$ ($j = 1, 2, \ldots, n$) is repulsive if $\epsilon_j > \epsilon_{j+1}$ and attractive if $\epsilon_j < \epsilon_{j+1}$ (with the convention $\epsilon_{n+1} = 0$). Particular cases of these discrete potentials when $n = 1$ are the popular square-well and square-shoulder potentials.

The phase diagram and the thermodynamic properties of discrete-potential fluids have been thoroughly examined and are relatively well understood.[4–16] On the other hand, studies of their structural properties either theoretical or from simulations are scarce.[10,17–21] In a previous paper,[19] following a semi-analytic methodology referred to generically as the rational-function approximation (RFA) that, although approximate, has proven successful for many other systems,[22] we derived the general formulae for the structural properties of fluids whose molecules interact via discrete potentials with a hard core plus an arbitrary number of piece-wise constant sections of different widths and heights. The theoretical scheme was illustrated by comparing it with available computer simulations results.[18]

The aim of this paper is to carry out a more systematic study of the structural properties of fluids characterized by a discrete potential with a hard core plus different combinations of a repulsive shoulder and an attractive well. This will be done by considering the results of Ref. 19 in the case of $n = 2$ for various values of the parameters and subsequently performing a comparison both with simulation results as well as with those that follow from the numerical solution of the Ornstein–Zernike (OZ) equation with both the Percus–Yevick (PY) and hypernetted-chain (HNC) closures. As will be seen, the performance of the RFA approach, despite its simplicity, is quite satisfactory.

The paper is organized as follows. In order to make it self-contained, in Sec. II we introduce the systems to be studied and sketch the derivation of the results of Ref. 19 for the structural properties of such systems when $n = 2$. We also include here some details of the simulation and of the numerical solution of the OZ equation with the PY and HNC closures. This is followed in Sec. III by the

[a)] Electronic mail: andres@unex.es; http://www.unex.es/eweb/fisteor/andres/

[b)] Electronic mail: santos@unex.es; http://www.unex.es/eweb/fisteor/santos/

[c)] Electronic mail: malopez@unam.mx; http://xml.cie.unam.mx/xml/tc/ft/mlh/

[d)] Electronic mail: mbarcenas@tese.edu.mx

[e)] Electronic mail: porea@imp.mx

comparison between the outcomes of the three different approaches for the radial distribution function (rdf). The paper is closed in Sec. IV with further discussion and some concluding remarks.

II. SYSTEM AND STRUCTURAL PROPERTIES

We consider a fluid of number density ρ and absolute temperature T in which the intermolecular pair potential is of the form of Eq. (1) with $n = 2$. We will take the hard-core diameter σ as the length unit so all distances will be measured in units of σ. The two main quantities usually employed to characterize the structure of fluids in equilibrium are the static structure factor $S(q)$ and the rdf $g(r)$ which are related by

$$S(q) = 1 + \rho \int dr\, e^{-i\mathbf{q}\cdot\mathbf{r}}[g(r) - 1] = 1 - 2\pi\rho\, \frac{G(s) - G(-s)}{s}\bigg|_{s=iq}, \tag{2}$$

where

$$G(s) = \int_0^\infty dr\, e^{-rs} r g(r) \tag{3}$$

is the Laplace transform of $rg(r)$.

A. The rational-function approximation method

We define an auxiliary function $F(s)$ directly related to $G(s)$ through

$$G(s) = s\frac{F(s)e^{-s}}{1 + 12\eta F(s)e^{-s}} = \sum_{m=1}^{\infty} (-12\eta)^{m-1} s[F(s)]^m e^{-ms}. \tag{4}$$

Here, $\eta = (\pi/6)\rho\sigma^3$ is the packing fraction. Laplace inversion of Eq. (4) provides a useful representation of $g(r)$, namely

$$g(r) = r^{-1} \sum_{m=1}^{\infty} (-12\eta)^{m-1} f_m(r - m)\Theta(r - m), \tag{5}$$

where $f_m(r)$ is the inverse Laplace transform of $s[F(s)]^m$ and $\Theta(r)$ is the Heaviside step function.

The contact value $g(1^+)$ of the rdf is related to $F(s)$ through $g(1^+) = f_1(0) = \lim_{s\to\infty} s^2 F(s)$ and it has to be finite. Further, as seen from Eq. (2), the behavior of $G(s)$ for small s determines the value of $S(0)$, which must also be finite. Hence, $F(s)$ must satisfy two conditions:[19]

$$F(s) \sim s^{-2}, \quad s \to \infty, \tag{6}$$

$$F(s) = -\frac{1}{12\eta}\left(1 + s + \frac{1}{2}s^2 + \frac{1+2\eta}{12\eta}s^3 + \frac{2+\eta}{24\eta}s^4\right) + \mathcal{O}(s^5). \tag{7}$$

Equations (4)–(7) are exact and valid for any interaction potential with a hard core at $r = \sigma = 1$. Now we particularize to the potential (1) with $n = 2$. To reflect the discontinuities of $g(r)$ at the points $r = \lambda_1$ and $r = \lambda_2$, where $\varphi(r)$ is discontinuous, we decompose $F(s)$ as

$$F(s) = R_0(s) + R_1(s)e^{-(\lambda_1-1)s} + R_2(s)e^{-(\lambda_2-1)s}. \tag{8}$$

As a consequence,

$$f_1(r) = \xi_0(r)\Theta(r) + \xi_1(r - \lambda_1 + 1)\Theta(r - \lambda_1 + 1) + \xi_2(r - \lambda_2 + 1)\Theta(r - \lambda_2 + 1), \tag{9}$$

where $\xi_j(r)$ denotes the inverse Laplace transform of $sR_j(s)$. If, as will be done here, one assumes that $\lambda_2 \le 2$, insertion of Eq. (9) into Eq. (5) gives the rdf in the shell $1 < r < 2$. In particular,

$$g(\lambda_1^-) = \lambda_1^{-1}\xi_0(\lambda_1 - 1), \tag{10}$$

$$g(\lambda_1^+) = \lambda_1^{-1}\left[\xi_0(\lambda_1 - 1) + \xi_1(0)\right], \tag{11}$$

$$g(\lambda_2^-) = \lambda_2^{-1}\left[\xi_0(\lambda_2 - 1) + \xi_1(\lambda_2 - \lambda_1)\right], \tag{12}$$

$$g(\lambda_2^+) = \lambda_2^{-1}\left[\xi_0(\lambda_2 - 1) + \xi_1(\lambda_2 - \lambda_1) + \xi_2(0)\right]. \tag{13}$$

Now we assume the following *rational-function* approximation for $R_j(s)$:

$$R_j(s) = -\frac{1}{12\eta}\frac{A_j + B_j s}{1 + S_1 s + S_2 s^2 + S_3 s^3}, \quad j = 0, 1, 2. \tag{14}$$

Note that Eq. (14) for $R_0(s)$ guarantees the fulfillment of the physical condition (6). Yet, the approximation (14) contains nine parameters to be determined. The exact expansion (7) imposes five constraints among those nine parameters, namely[19]

$$1 = A_0 + A_1 + A_2, \tag{15}$$

$$S_1 = -1 + B_0 - C^{(1)}, \tag{16}$$

$$S_2 = \frac{1}{2} - B_0 + C^{(1)} + \frac{1}{2}C^{(2)}, \tag{17}$$

$$S_3 = -\frac{1+2\eta}{12\eta} + \frac{1}{2}B_0 - \frac{1}{2}C^{(1)} - \frac{1}{2}C^{(2)} - \frac{1}{6}C^{(3)}, \tag{18}$$

$$B_0 = C^{(1)} + \frac{\eta/2}{1+2\eta}\left(6C^{(2)} + 4C^{(3)} + C^{(4)}\right) + \frac{1+\eta/2}{1+2\eta}. \tag{19}$$

Here,

$$C^{(k)} \equiv \sum_{j=1}^{2}\left[A_j(\lambda_j - 1)^k - kB_j(\lambda_j - 1)^{k-1}\right]. \tag{20}$$

Next, since the cavity function $y(r) \equiv g(r)e^{\beta\varphi(r)}$, where $\beta \equiv 1/k_BT$ (k_B being the Boltzmann constant), must be continuous at $r = \lambda_1$ and $r = \lambda_2$, one obtains from Eqs. (10)–(13) the two conditions[19]

$$\frac{B_1}{S_3} = \left[e^{\beta(\epsilon_1-\epsilon_2)} - 1\right] \sum_{\alpha=1}^{3} \frac{s_\alpha e^{(\lambda_1-1)s_\alpha}}{S_1 + 2S_2 s_\alpha + 3S_3 s_\alpha^2} \times (A_0 + B_0 s_\alpha), \tag{21}$$

$$\frac{B_2}{S_3} = \left(e^{\beta\epsilon_2} - 1\right) \sum_{\alpha=1}^{3} \frac{s_\alpha e^{(\lambda_2-1)s_\alpha}}{S_1 + 2S_2 s_\alpha + 3S_3 s_\alpha^2} \times \left[A_0 + B_0 s_\alpha + (A_1 + B_1 s_\alpha) e^{-(\lambda_1-1)s_\alpha}\right], \tag{22}$$

where s_α ($\alpha = 1, 2, 3$) are the three roots of the cubic equation

$$1 + S_1 s_\alpha + S_2 s_\alpha^2 + S_3 s_\alpha^3 = 0. \tag{23}$$

Equations (15)–(19), (21), and (22) still leave two parameters undetermined. A simplifying assumption is that the coefficients A_j ($j = 0, 1, 2$) may be fixed at their zero-density values, namely

$$A_0 = e^{-\beta\epsilon_1}, \quad A_1 = e^{-\beta\epsilon_2} - e^{-\beta\epsilon_1}, \quad A_2 = 1 - e^{-\beta\epsilon_2}. \tag{24}$$

This closes the problem of determining the nine parameters in terms of η, λ_1, λ_2, $\beta\epsilon_1$, and $\beta\epsilon_2$. In fact, Eqs. (16)–(19) allow us to express S_1, S_2, S_3, and B_0 as linear combinations of B_1 and B_2, so that in the end one only has to solve (numerically) the two coupled transcendental equations (21) and (22). Since the dependence of $G(s)$ on s is explicit, we are now in a position to compute the structural quantities of our systems. The structure factor $S(q)$ can be directly obtained from Eq. (2), while the rdf $g(r)$ can be obtained from Eq. (5) or, more directly, by numerical inverse Laplace transform of $G(s)$.[23]

B. The PY and HNC approximations

In the usual integral equation approach to the theory of liquids, the OZ equation, which may be formally considered as a definition of the direct correlation function $c(r)$, provides a link between this direct correlation function and the total correlation function $h(r) \equiv g(r) - 1$, the latter being a measure of the 'influence', either direct or through a third molecule, of two molecules separated a distance r away. The OZ relation reads

$$h(r) = c(r) + \rho \int d\mathbf{r}' c(r') h(|\mathbf{r} - \mathbf{r}'|) = c(r) + \frac{2\pi\rho}{r} \int_0^\infty dr'\, r' c(r') \int_{|r-r'|}^{r+r'} dr''\, r'' h(r''), \tag{25}$$

where in the second equality we have particularized to three-dimensional systems and used bipolar coordinates.[24,25]

Since both $h(r)$ and $c(r)$ are unknown, in order to close the description one requires an additional equation, known as the closure relation. A closure can be expressed as a local relationship between the direct correlation function and the Mayer function $f(r) \equiv e^{-\beta\varphi(r)} - 1$ and the cavity function $y(r)$, i.e.,

$$c(r) = \mathcal{C}\left(f(r), y(r)\right). \tag{26}$$

Equivalently, Eq. (26) can be inverted to obtain a local relationship between the cavity function and the indirect correlation function $\gamma(r) \equiv h(r) - c(r)$, i.e.,

$$y(r) = \mathcal{Y}\left(\gamma(r)\right). \tag{27}$$

Insertion of the closure (26) and (27) into the OZ relation (25) yields a closed nonlinear integral equation for the cavity function:

$$y(r) = \mathcal{Y}\left(\frac{2\pi\rho}{r} \int_0^\infty dr'\, r' \mathcal{C}\left(f(r'), y(r')\right) \times \int_{|r-r'|}^{r+r'} dr''\, r'' \left[e^{-\beta\varphi(r'')} y(r'') - 1\right]\right). \tag{28}$$

As mentioned in Sec. I, we will consider here both the PY and HNC closures given by

$$c(r) = h(r) - y(r) + 1 \quad \text{(PY)}, \tag{29}$$

$$c(r) = h(r) - \ln y(r) \quad \text{(HNC)}. \tag{30}$$

In terms of the functions $\mathcal{C}(f, y)$ and $\mathcal{Y}(\gamma)$, the PY and HNC closure relations are

$$\mathcal{C}(f, y) = fy, \quad \mathcal{Y}(\gamma) = 1 + \gamma \quad \text{(PY)}, \tag{31}$$

$$\mathcal{C}(f, y) = (f+1)y - 1 - \ln y, \quad \mathcal{Y}(\gamma) = e^\gamma \quad \text{(HNC)}. \tag{32}$$

We have solved Eq. (28) numerically in the PY and HNC cases. First, a discretization scheme $y(r) \to \{r_i, y_i\}$ with $r_i = i\Delta r$ ($i = 1, 2, \ldots, \mathcal{N}$) and a cut-off distance $r_\mathcal{N} = \mathcal{N}\Delta r$ are introduced, so that the integral equation (28) is replaced by a set of $\mathcal{N}$ nonlinear coupled equations:

$$y_i = \mathcal{Y}\left(\frac{2\pi\rho}{r_i}(\Delta r)^2 \sum_{j=1}^{\mathcal{N}} r_j \mathcal{C}\left(f_j, y_j\right) \times \sum_{k=|i-j|+1}^{\min(i+j,\mathcal{N})} r_k \left(e^{-\beta\varphi_k} y_k - 1\right)\right), \quad i = 1, 2, \ldots, \mathcal{N}. \tag{33}$$

Next, a coarse-grained solution of Eq. (33) is obtained by an iteration method. Insertion of the nth order input $\{y_i^{(n,\text{in})}\}$ into the right-hand side of Eq. (33) gives the nth order output $\{y_i^{(n,\text{out})}\}$ and the subsequent input is constructed as $y_i^{(n+1,\text{in})} = \alpha y_i^{(n,\text{out})} + (1-\alpha) y_i^{(n,\text{in})}$, with

a convenient choice of the mixing parameter α. The iterations are continued until the convergence criterion

$$\max_i |y_i^{(n,\text{out})} - y_i^{(n,\text{in})}| < 10^{-3} \tag{34}$$

is reached or the number of iterations exceeds 100. Once the coarse-grained solution has been obtained, a fine-grained solution of the set of $\mathcal{N}$ equations (33) is determined with the help of a computational software program, using the coarse-grained solution as a seed.[26] In the numerical solutions presented in Sec. III we have generally used $\Delta r = 0.01\sigma$ and $\mathcal{N} = 400$. As for the mixing parameter α, it was chosen by trial and error, being necessary to decrease it as the density increases.

C. Technical simulation details

The simulation data were computed with a Replica Exchange Monte Carlo (REMC) method. The REMC method is also known as Parallel Tempering and was derived to achieve good sampling of systems that present a free energy landscape with many local minima.[27] The REMC method consists of simulating M replicas (copies) of the system at different thermodynamic conditions; the attempted MC moves are accepted or rejected according to the traditional Metropolis algorithm. Due to these exchanges, a particular replica travels through many temperatures, allowing it to overcome any barriers to free energy.

The method samples an expanded canonical ensemble, taking the temperature as the expansion variable. The existence of this expanded ensemble justifies the introduction of movements of exchange between replicas. The expanded ensemble is defined as

$$Q_{\text{expanded}} = \prod_{i=1}^{M} Q_i, \tag{35}$$

where Q_i is the partition function of the (NVT) canonical ensemble of the system (subensemble i) at temperature T, volume V, and number of particles N. To satisfy the detailed balance condition, the probability of acceptance of the exchange is given by

$$P_{\text{acc}} = \min(1, \exp[-(\beta_j - \beta_i)(U_j - U_i)]), \tag{36}$$

where $\beta_j - \beta_i$ is the difference between the reciprocal temperatures and $U_j - U_i$ is the difference between the potential energies of the subensembles i and j.

A cubic simulation box of dimensions $L_x = L_y = L_z = 10\sigma$ was used and periodic boundary conditions were set in the three directions. Verlet lists[28] were implemented to improve performance. We have carried out computer experiments for different systems, corresponding to different values of the parameters of the potentials that will be specified later. These systems are further characterized by their reduced density $\rho^* = \rho\sigma^3$ and their reduced temperature $T^* = k_BT/\epsilon$, where $\epsilon = \max(|\epsilon_1|, |\epsilon_2|)$. The number of replicas $M = 12$ was chosen to match the number of different temperatures in which we want to examine the systems. The highest temperature was set at $T^* = 2$, while the other temperatures were established following a decreasing geometric progression, namely $T_n^* = 2(0.959)^{n-1}$, $n = 1, \ldots, 12$. The initial configuration of each system, consisting of a collection of $N = 500$ particles randomly arranged in the simulation box and thus setting the reduced number density of our systems as $\rho^* = 0.5$, was equilibrated by conducting 10^7 Monte Carlo simulation steps. The rdf was calculated over additional 4×10^7 configurations.

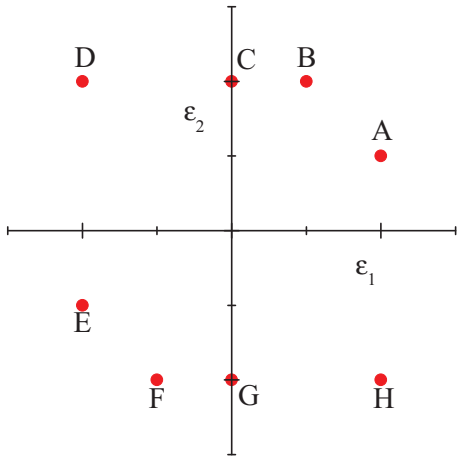

FIG. 1. (Color online). Diagram in the ϵ_2–ϵ_1 plane illustrating the choices of the values corresponding to the eight different cases to be studied, labeled from A to H.

III. RESULTS

For convenience and in order to try to be systematic, we now first fix the values of λ_1 and λ_2 to be $\lambda_1 = 1.25$ and $\lambda_2 = 1.5$. As for the values of ϵ_1 and ϵ_2 we have considered the eight representative cases sketched in Fig. 1. At this stage some comments are in order. Since, as already stated, $\epsilon = \max(|\epsilon_1|, |\epsilon_2|)$, at least one of the $|\epsilon_i|$ must be equal to ϵ. The other energy level has been chosen as 0, $\pm\epsilon$, or $\pm\frac{1}{2}\epsilon$ with the following conditions. First, the cases having $\epsilon_1 = \epsilon_2$ have not been considered since they correspond to having just one step. The same can be said about the cases with $\epsilon_2 = 0$. Finally, if ϵ_1 and ϵ_2 have opposite signs, then we have taken $|\epsilon_1| = |\epsilon_2| = \epsilon$. The potentials of the different cases (from A to H) are represented graphically in Fig. 2. We observe that system A corresponds to a purely repulsive potential. In the cases B–D the potential is repulsive at $r/\sigma = \lambda_2$ and attractive at $r/\sigma = \lambda_1$, with increasing attraction when going from B to D. System E presents a purely attractive tail beyond the hard core. As for systems F–H, the potential is attractive at $r/\sigma = \lambda_2$ and repulsive at

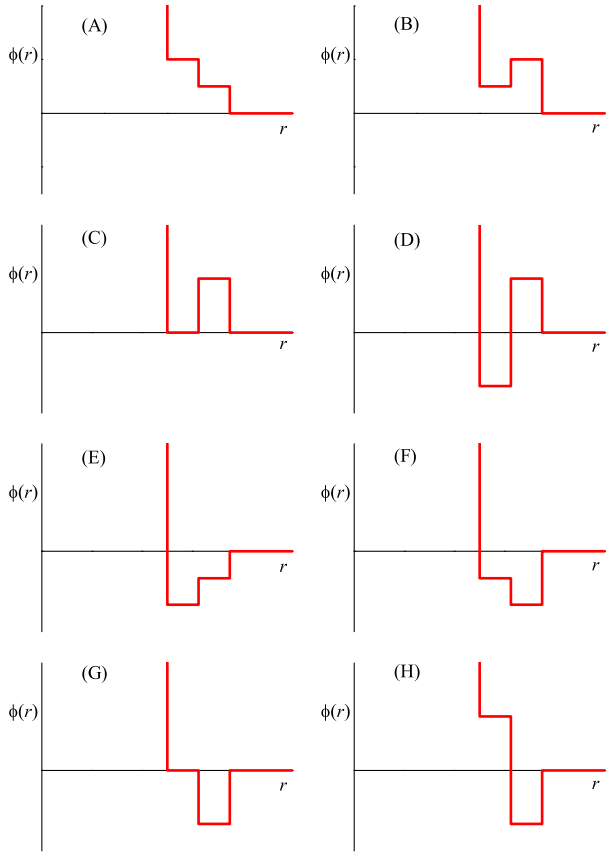

FIG. 2. (Color online). Diagrams of the surveyed potentials, labeled from A to H.

$r/\sigma = \lambda_1$, with increasing repulsion when going from F to H. The cases A and F–H are examples of core-softened potentials.

As an illustration of the results of our calculations, and in accordance with the simulation experiments mentioned above, we fix the reduced density to be $\rho^* = 0.5$ and consider the lowest reduced temperature $T^* = 1.26193$ (corresponding to $n = M = 12$) in all cases, although, as said before, we obtained simulation data for the whole temperature range $1.26193 \leq T^* \leq 2$. The results for the rdf are displayed in Figs. 3–10 for cases A–H, respectively. In order to assess the influence of ϵ_1 and ϵ_2 on $g(r)$ at fixed (reduced) temperature and density, common horizontal and vertical scales have been chosen in Figs. 3–10. In the case of the purely repulsive system A, there exists a local accumulation of particles at the external edge (λ_i^+) of each repulsive step, followed by a local depletion at the internal edge (λ_i^-). For systems B–D, where the potential is repulsive at $r/\sigma = \lambda_2$ but attractive at $r/\sigma = \lambda_1$, the population of particles (as seen by a reference particle at the origin) is depleted in the region $\lambda_1 < r/\sigma < \lambda_2$ and increases when going from λ_1^+ to λ_1^-, as expected. These effects are enhanced as the depth of the inner well increases. In the case of system E the potential outside the hard core is purely attractive, what is reflected in an increase of $g(r)$ from the external edge λ_i^+ to the internal edge λ_i^-. Finally, systems F–H are the counterparts of systems B–D. Now the attraction at $r/\sigma = \lambda_2$ produces an increase of particles in the region $\lambda_1 < r/\sigma < \lambda_2$, this effect being enhanced as the inner barrier becomes more repulsive. Interestingly enough, the correlation length, i.e., the distance beyond which $|g(r) - 1|$ is lower than a certain small value, in-

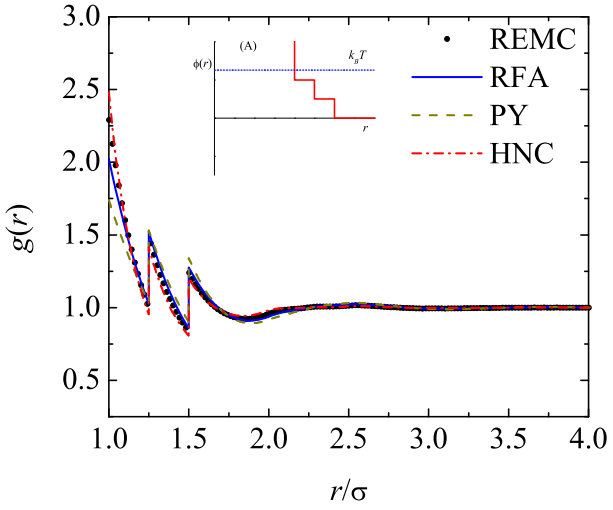

FIG. 3. (Color online). Comparison of the different theoretical approaches to compute the rdf of the system corresponding to case A ($\lambda_1 = 1.25$, $\lambda_2 = 1.5$, $\epsilon_1 = \epsilon$, $\epsilon_2 = \epsilon/2$) at $\rho^* = 0.5$ and $T^* = 1.26193$ with simulation results. Solid line: RFA; dashed line: HNC; dotted-dashed line: PY; symbols: REMC data. The inset shows the interaction potential and the temperature value.

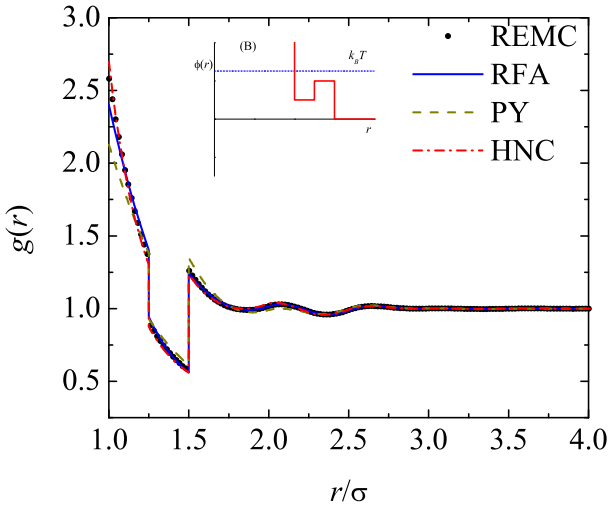

FIG. 4. (Color online). Comparison of the different theoretical approaches to compute the rdf of the system corresponding to case B ($\lambda_1 = 1.25$, $\lambda_2 = 1.5$, $\epsilon_1 = \epsilon/2$, $\epsilon_2 = \epsilon$) at $\rho^* = 0.5$ and $T^* = 1.26193$ with simulation results. Solid line: RFA; dashed line: HNC; dotted-dashed line: PY; symbols: REMC data. The inset shows the interaction potential and the temperature value.

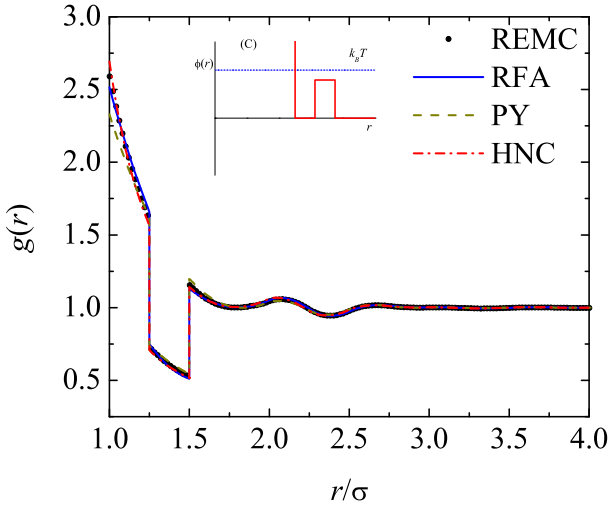

FIG. 5. (Color online). Comparison of the different theoretical approaches to compute the rdf of the system corresponding to case C ($\lambda_1 = 1.25$, $\lambda_2 = 1.5$, $\epsilon_1 = 0$, $\epsilon_2 = \epsilon$) at $\rho^* = 0.5$ and $T^* = 1.26193$ with simulation results. Solid line: RFA; dashed line: HNC; dotted-dashed line: PY; symbols: REMC data. The inset shows the interaction potential and the temperature value.

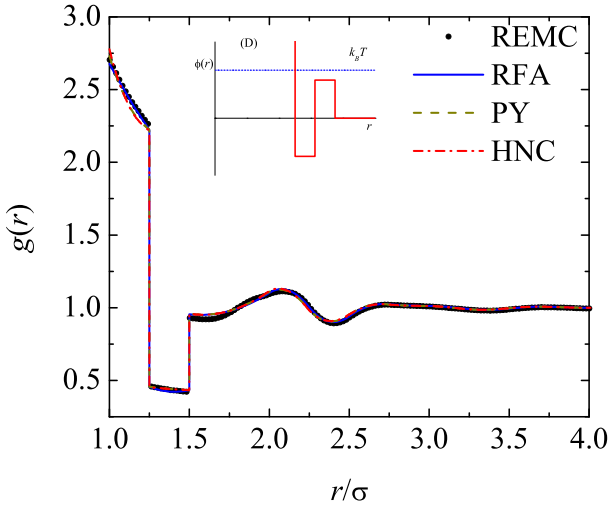

FIG. 6. (Color online). Comparison of the different theoretical approaches to compute the rdf of the system corresponding to case D ($\lambda_1 = 1.25$, $\lambda_2 = 1.5$, $\epsilon_1 = -\epsilon$, $\epsilon_2 = \epsilon$) at $\rho^* = 0.5$ and $T^* = 1.26193$ with simulation results. Solid line: RFA; dashed line: HNC; dotted-dashed line: PY; symbols: REMC data. The inset shows the interaction potential and the temperature value.

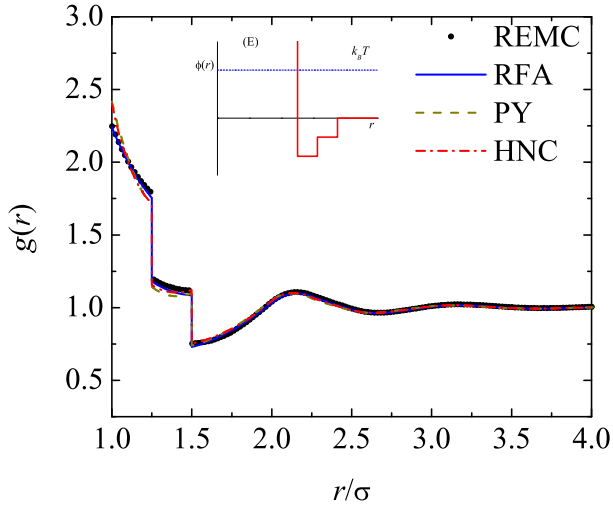

FIG. 7. (Color online). Comparison of the different theoretical approaches to compute the rdf of the system corresponding to case E ($\lambda_1 = 1.25$, $\lambda_2 = 1.5$, $\epsilon_1 = -\epsilon$, $\epsilon_2 = -\epsilon/2$) at $\rho^* = 0.5$ and $T^* = 1.26193$ with simulation results. Solid line: RFA; dashed line: HNC; dotted-dashed line: PY; symbols: REMC data. The inset shows the interaction potential and the temperature value.

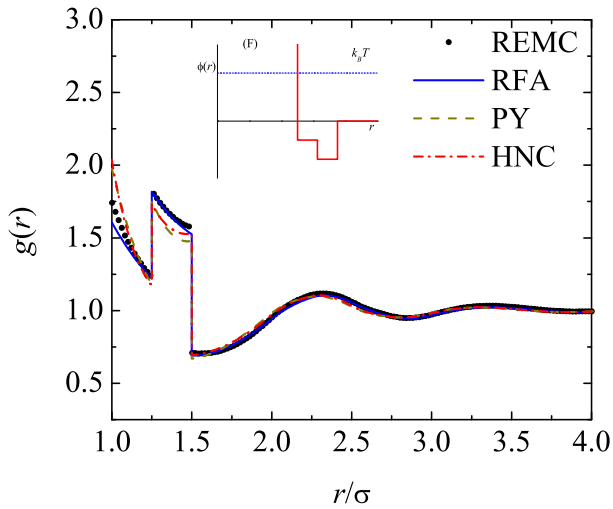

FIG. 8. (Color online). Comparison of the different theoretical approaches to compute the rdf of the system corresponding to case F ($\lambda_1 = 1.25$, $\lambda_2 = 1.5$, $\epsilon_1 = -\epsilon/2$, $\epsilon_2 = -\epsilon$) at $\rho^* = 0.5$ and $T^* = 1.26193$ with simulation results. Solid line: RFA; dashed line: HNC; dotted-dashed line: PY; symbols: REMC data. The inset shows the interaction potential and the temperature value.

creases monotonically from system A (Fig. 3) to system H (Fig. 10).

Let us comment now on the theoretical predictions. It follows that, as already pointed out in Ref. 19, the RFA approach certainly outperforms the PY approximation in all the cases. This is noteworthy because, while the RFA reduces to the PY solution for hard spheres,[19] it is much simpler than the PY integral equation theory for two-step potentials. As for the HNC integral equation theory, it presents the best agreement in the region $1 < r/\sigma < \lambda_1$ in the cases A–C, i.e., when $\epsilon_1 \geq 0$ and $\epsilon_2 > 0$. Even in those cases, however, the RFA is as accurate as or more accurate than the HNC theory in the region $\lambda_1 < r/\sigma < \lambda_2$. For larger distances the RFA and HNC

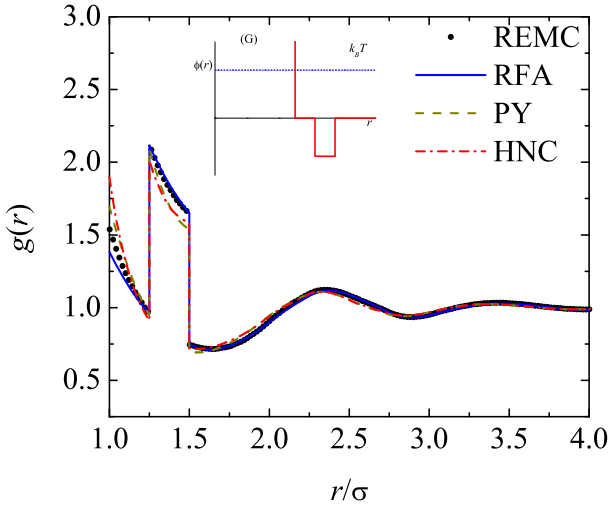

FIG. 9. (Color online). Comparison of the different theoretical approaches to compute the rdf of the system corresponding to case G ($\lambda_1 = 1.25$, $\lambda_2 = 1.5$, $\epsilon_1 = 0$, $\epsilon_2 = -\epsilon$) at $\rho^* = 0.5$ and $T^* = 1.26193$ with simulation results. Solid line: RFA; dashed line: HNC; dotted-dashed line: PY; symbols: REMC data. The inset shows the interaction potential and the temperature value.

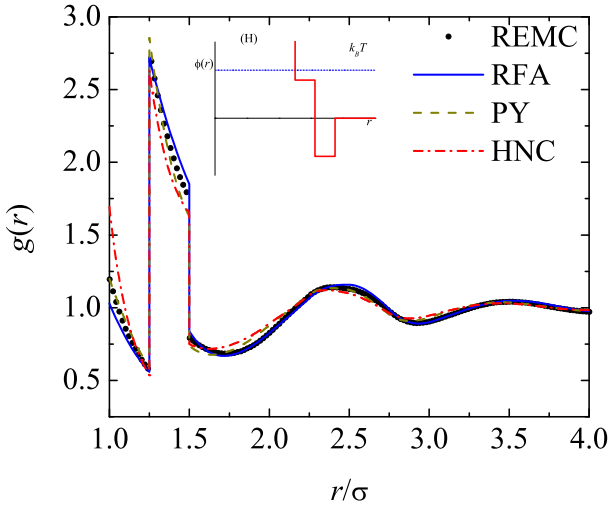

FIG. 10. (Color online). Comparison of the different theoretical approaches to compute the rdf of the system corresponding to case H ($\lambda_1 = 1.25$, $\lambda_2 = 1.5$, $\epsilon_1 = \epsilon$, $\epsilon_2 = -\epsilon$) at $\rho^* = 0.5$ and $T^* = 1.26193$ with simulation results. Solid line: RFA; dashed line: HNC; dotted-dashed line: PY; symbols: REMC data. The inset shows the interaction potential and the temperature value.

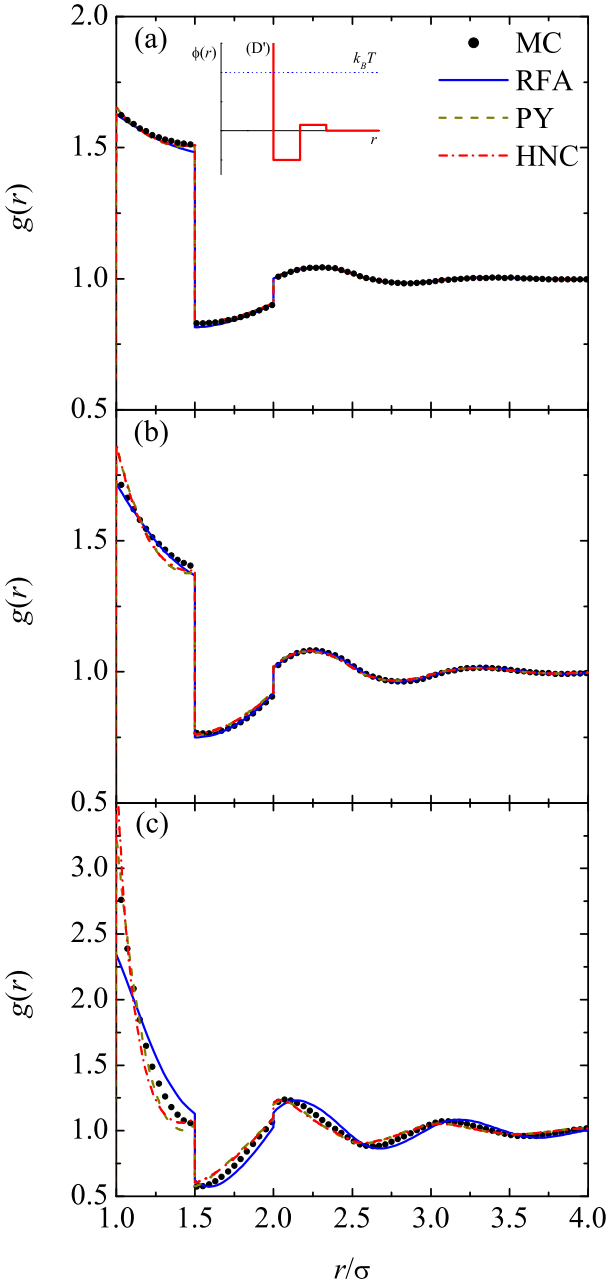

FIG. 11. (Color online).Comparison of the different theoretical approaches to compute the rdf of the system corresponding to case D' ($\lambda_1 = 1.5$, $\lambda_2 = 2$, $\epsilon_1 = -\epsilon$, $\epsilon_2 = \epsilon/5$) at $T^* = 2$ and (a) $\rho^* = 0.2$, (b) $\rho^* = 0.4$, and (c) $\rho^* = 0.75$ with simulation results. Solid line: RFA; dashed line: HNC; dotted-dashed line: PY; symbols: MC data.[17] The inset shows the interaction potential and the temperature value.

predictions are almost indistinguishable. In the rest of the cases (D–H), the PY and HNC curves are generally very similar, the best global performance being obtained with the RFA.

As a final illustration, we present in Figs. 11 and 12 a comparison of the results we have obtained with the different theoretical approaches with those of MC simulations[17] of two systems with an intermolecular potential of the type of case D (square well + square barrier), but this time having the following values of the parameters: $\lambda_1 = 1.5$, $\lambda_2 = 2$, $\epsilon_1 = -\epsilon$, $\epsilon_2 = \epsilon/5$ (system D') and $\lambda_1 = 1.5$, $\lambda_2 = 2$, $\epsilon_1 = -\epsilon$, $\epsilon_2 = 2\epsilon/5$ (system D"), respectively. For those systems we have considered a fixed temperature $T^* = 2$ and the three reduced densities

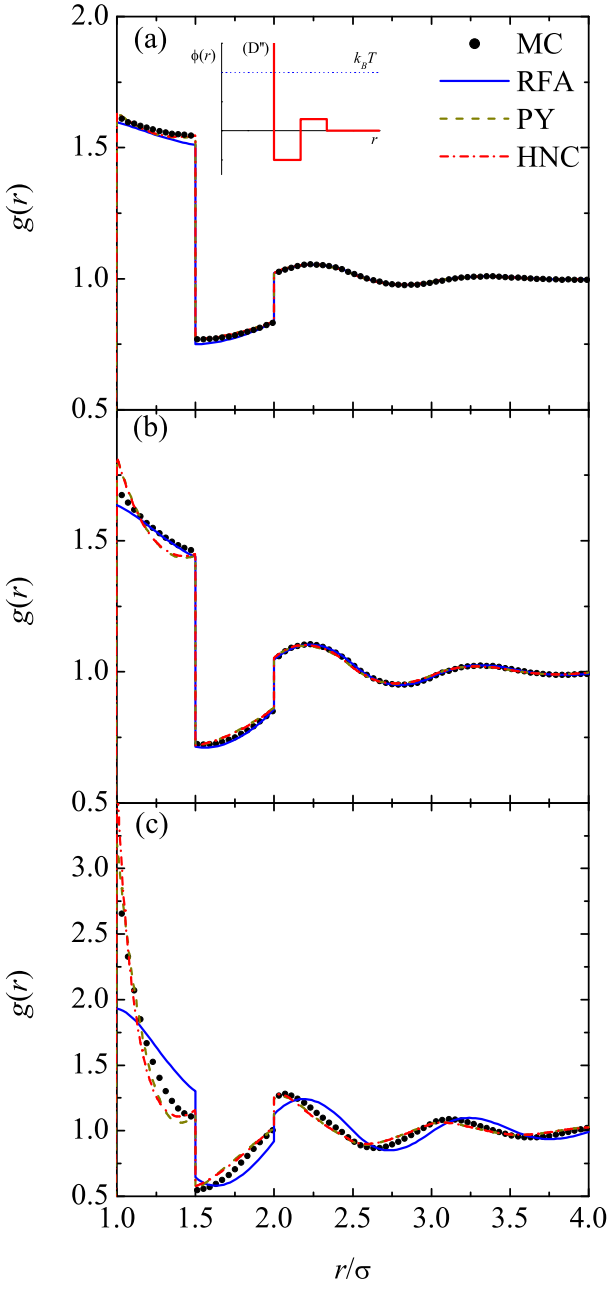

FIG. 12. (Color online).Comparison of the different theoretical approaches to compute the rdf of the system corresponding to case D" ($\lambda_1 = 1.5$, $\lambda_2 = 2$, $\epsilon_1 = -\epsilon$, $\epsilon_2 = 2\epsilon/5$) at $T^* = 2$ and (a) $\rho^* = 0.2$, (b) $\rho^* = 0.4$, and (c) $\rho^* = 0.75$ with simulation results. Solid line: RFA; dashed line: HNC; dotted-dashed line: PY; symbols: MC data.[17] The inset shows the interaction potential and the temperature value.

$\rho^* = 0.2$, $\rho^* = 0.4$, and $\rho^* = 0.75$.[29] At the lowest density ($\rho^* = 0.2$) the three theoretical approaches provide excellent results, with a slight superiority of PY and HNC. At the intermediate density ($\rho^* = 0.4$), however, the RFA beats the PY and HNC results (which are practically indistinguishable from each other). Finally, at the highest density ($\rho^* = 0.75$) the RFA becomes clearly worse than the PY and HNC predictions (which are again hardly distinguishable), especially in the case of the higher barrier (case D").

IV. CONCLUDING REMARKS

In this paper we have presented a rather systematic study of the rdf of fluids whose molecules interact via a potential with a hard core plus two piece-wise constant sections of the same width and different heights (either wells or shoulders), which include the RFA approach, our own REMC numerical experiments, and the numerical solution of the PY and HNC integral equations. We have considered eight representative classes of systems (see Figs. 1 and 2) which cover all the possible topologies of hard core plus two-step potentials. They include a purely repulsive potential (system A), potentials with an outer repulsive barrier and an inner attractive well (systems B–D), a purely attractive part outside the hard core (system E), and potentials with an outer attractive well and an inner repulsive barrier (systems F–H). Four of these systems (A and F–H) belong to the class of core-softened potentials.

As Figs. 3–10 show, it is fair to state that for the fixed number density $\rho^* = 0.5$ the agreement between the results of our RFA formulation and those of the REMC experiments is very satisfactory in all instances. This is specially rewarding in view of the fact that the reduced temperature we have chosen to illustrate our findings ($T^* = 1.26193$) is rather low and represents a stringent test of our theory.

We have complemented our study with the comparison of the results we get and the MC data of Ref. 17 for two cases (labeled here as D' and D") in which the potential is of the form of the one of case D but with a wider width, a lower outer barrier, and a fixed reduced temperature $T^* = 2$. Again, as observed from Figs. 11 and 12, the performance of the RFA approach is rather satisfactory, except at the highest density $\rho^* = 0.75$. The tendency of the RFA to fail at high densities and wide potentials widths was already documented in the case of the pure square-well potential (with $\epsilon_2 = 0$).[30]

Concerning the comparison between our present approach and the usual integral equation approach in the theory of liquids, we have seen that the RFA is rather simple, requires much less numerical labor (in these cases only the solution of two coupled transcendental equations), captures correctly all the oscillations of the rdf, and is reasonably accurate. In fact, it is always superior to the PY equation [except for the cases of Figs. 11(c) and 12(c)] and in most of the instances it is of comparable accuracy or better than the HNC equation. Hence, this constitutes further evidence of the usefulness of the RFA methodology that we have used for the computation of the structural properties of different hard-core fluids.[22]

As a final point, we want to stress that the results of this paper, together with the earlier ones,[19] encour-

age us to consider the problem in which the number of steps in the potential is much greater, leading in the limit $n \to \infty$ to the very interesting case of the structure in a fluid whose molecules interact via, for instance, a Jagla potential. We plan to undertake such a task in the future.

ACKNOWLEDGMENTS

We want to thank R. Castañeda-Priego and S. P. Hlusak for kindly supplying us with all the simulation data of Refs. 10 and 17, respectively. Two of us (A.S. and S.B.Y) acknowledge the financial support of the Spanish Government through Grant No. FIS2010-16587 and the Junta de Extremadura (Spain) through Grant No. GR10158 (partially financed by FEDER funds). P.O. thanks the Molecular Engineering Program of IMP.

[1] G. A. Chapela, S. E. Martínez-Casas, and J. Alejandre, Mol. Phys. **53**, 139 (1984).
[2] P. T. Cummings and G. Stell, Mol. Phys. **51**, 253 (1984).
[3] G. A. Chapela, L. E. Scriven, and H. T. Davis, J. C **91**, 4307 (1989).
[4] A. L. Benavides and A. Gil-Villegas, Mol. Phys. **97**, 1225 (1999).
[5] A. Vidales, A. L. Benavides, and A. Gil-Villegas, Mol. Phys. **99**, 703 (2001).
[6] G. Franzese, G. Malescio, A. Skibinsky, S. V. Buldyrev, and H. E. Stanley, Nature **409**, 692 (2001).
[7] A. Skibinsky, S. V. Buldyrev, G. Franzese, G. Malescio, and H. E. Stanley, Phys. Rev. E **69**, 061206 (2004).
[8] G. Malescio, G. Franzese, A. Skibinsky, S. V. Buldyrev, and H. E. Stanley, Phy. Rev. E **71**, 061504 (2005).
[9] A. L. Benavides, L. A. del Pino, A. Gil-Villegas, and F. Sastre, J. Chem. Phys. **125**, 204715 (2006).
[10] I. Guillén-Escamilla, M. Chávez-Páez, and R. Castañeda-Priego, J. Phys.: Cond. Matt. **19**, 086224 (2007).
[11] L. A. Cervantes, A. L. Benavides, and F. del Río, J. Chem. Phys. **126**, 084507 (2007).
[12] A. B. de Oliveira, G. Franzese, P. A. Netz, and M. C. Barbosa, J. Chem. Phys. **128**, 064901 (2008).
[13] W. Rżysko, O. Pizio, A. Patrykiejew, and S. Sokolowski, J. Chem. Phys. **129**, 124502 (2008).
[14] A. B. de Oliveira, P. A. Netz, and M. C. Barbosa, Europhys. Lett. **85**, 36001 (2009).
[15] W. Rżysko, A. Patrykiejew, S. Sokołowski, and O. Pizio, J. Chem. Phys. **132**, 164702 (2010).
[16] Y. D. Fomin, E. N. Tsiok, and V. N. Ryzhov, J. Chem. Phys. **134**, 044523 (2010).
[17] S. P. Hlushak, A. D. Trokhymchuk, and S. Sokołowski, J. Chem. Phys. **134**, 114101 (2011).
[18] M. Bárcenas, G. Odriozola, and P. Orea, Rev. Mex. Fís. **57**, 485 (2011).
[19] A. Santos, S. B. Yuste, and M. López de Haro, Condens. Matter Phys. **15**, 23602 (2012).
[20] A. Loredo-Osti and R. Castañeda-Priego, J. Nanofluids **1**, 36 (2012).
[21] M. Bárcenas, G. Odriozola, and P. Orea, J. Mol. Liq. (2012), URL `http://www.sciencedirect.com/science/article/pii/S0167732212003856`.
[22] M. López de Haro, S. B. Yuste, and A. Santos, in *Theory and Simulation of Hard-Sphere Fluids and Related Systems*, edited by A. Mulero (Springer-Verlag, Berlin, 2008), vol. 753 of *Lectures Notes in Physics*, pp. 183–245.
[23] J. Abate and W. Whitt, Queueing Systems **10**, 5 (1992).
[24] A. A. Broyles, J. Chem. Phys. **35**, 493 (1961).
[25] A. Ben-Naim and V. K. Shen, J. Chem. Phys. **129**, 194514 (2008).
[26] More specifically, we have used the command FindRoot of Mathematica.
[27] G. Odriozola, F. Jiménez-Ángeles, and P. Orea, Chem. Phys. Lett. **501**, 466 (2011).
[28] L. Verlet, Phy. Rev. **159**, 98 (1967).
[29] Completely similar systems were considered in Ref. 10 but for different reduced densities. For brevity and because they are more recent, we decided to present here only the comparison with the results of Ref. 17. However, we have also performed a comparison between our results and the former MC data and this comparison is available upon request.
[30] S. B. Yuste and A. Santos, J. Chem. Phys. **101**, 2355 (1994).